

- (6) D. C. Bradley and K. J. Fisher, *MTP Int. Rev. Sci., Ser. One*, **5**, 65 (1972).
- (7) Allyl and benzyl compounds of the type ML_4 are known; see ref 2 and 3.
- (8) D. C. Bradley and M. H. Chisholm, *J. Chem. Soc. A*, 1511 (1971).
- (9) E. C. Alyea, J. S. Basl, D. C. Bradley, and M. H. Chisholm, *J. Chem. Soc. A*, 772 (1971).
- (10) G. Kyrkaez and R. J. Rocek, *J. Am. Chem. Soc.*, **95**, 4756 (1973).
- (11) Alkoxides are known to undergo adduct formation with Lewis basis such as amines, e.g., $[Nb(OMe)_5]_2 + 2L \rightleftharpoons 2Nb(OMe)_5L$, and $Mo_2(OR)_6 + 2L \rightleftharpoons Mo_2(OR)_6L_2$: M. H. Chisholm, F. A. Cotton, C. A. Murillo, and W. W. Reichert, *J. Am. Chem. Soc.*, **99**, 1652 (1977); *Inorg. Chem.*, **18**, 1801 (1977).
- (12) D. C. Bradley and I. M. Thomas, *J. Chem. Soc.*, 3404 (1959).
- (13) D. C. Bradley and M. M. Faktor, *Trans. Faraday Soc.*, 2117 (1959).
- (14) J. A. Ibers, *Nature (London)*, **197**, 686 (1963).
- (15) D. C. Bradley and C. E. Hollaway, *Inorg. Chem.*, **3**, 1163 (1964).
- (16) D. C. Bradley and C. E. Hollaway, *J. Chem. Soc. A*, 1316 (1968).
- (17) W. R. Russo and W. H. Nelson, *J. Am. Chem. Soc.*, **92**, 1521 (1970).
- (18) D. F. Evans, *J. Chem. Soc.*, 2003 (1959).
- (19) B. N. Figgis in "Introduction to Ligand Fields," Interscience, New York, N.Y., 1966.
- (20) F. A. Cotton, *Acc. Chem. Res.*, **2**, 240 (1968); *Chem. Soc. Rev.*, **4**, 27 (1975). The molecular structure of $Mo_2(OPr-i)_6$ has been deduced from x-ray studies. The molecule has rigorous inversion symmetry and virtual C_{2h} symmetry and there is essentially trigonal bipyramidal coordination about each molybdenum atom. The central planar $Mo_2(\mu-O)_2$ moiety is made from bridging isopropoxy ligands which form alternately long (axial) and short (equatorial) Mo-O bonds. The Mo-Mo distance is 2.525 (1) Å indicative of a Mo-to-Mo double bond which may be considered to arise from overlap of a metal $d_{xz} - d_{yz}$ and $d_{yz} - d_{xz}$ orbitals. Thus in a formal sense the double bond is comprised of a σ and a δ bond. F. A. Cotton and M. W. Extine, private communication.
- (21) MoO_2 has a rutile-like structure but is distorted by the presence of Mo-Mo bonds (2.51 Å): B. G. Brandt and A. C. Skapski, *Acta Chem. Scand.*, **21**, 661 (1967).
- (22) W. H. McCarroll, L. Katz, and R. Ward, *J. Am. Chem. Soc.*, **79**, 5410 (1957).
- (23) M. H. Chisholm, F. A. Cotton, C. A. Murillo, and W. W. Reichert, *Inorg. Chem.*, **16**, 1801 (1977).
- (24) M. H. Chisholm, F. A. Cotton, M. W. Extine, and W. W. Reichert, *J. Am. Chem. Soc.*, **100**, 153 (1978).
- (25) Molecular Structure Corp., P.O. Box DF, College Station, Texas.
- (26) Crystal data: triclinic; space group $P1$; $a = 9.661$ (2), $b = 9.863$ (3), $c = 9.419$ (5) Å, $V = 766.8$ (5) Å³, $\lambda = 0.710$ 73, $\alpha = 115.29$ (2)⁰, $\beta = 108.92$ (2), $\gamma = 84.33$ (2)⁰, $d_{calcd} = 1.175$ g/cm³; $M = 542.87$; $Z = 1$. For full crystallographic details see paragraph at end of paper regarding supplementary material.
- (27) W. Mowat, A. J. Shortland, N. J. Hill, and G. Wilkinson, *J. Chem. Soc., Dalton Trans.* 770 (1973).
- (28) F. Huq, W. Mowat, A. C. Skapski, and G. Wilkinson, *Chem. Commun.*, 1477 (1971).
- (29) M. H. Chisholm, W. W. Reichert, R. G. Anderson, G. Wilkinson, and J. F. Gibson, results to be published.
- (30) L. H. Sommer, E. W. Pietrusza, and F. C. Whitmore, *J. Am. Chem. Soc.*, **68**, 2282 (1946).
- (31) For details of the equipment see M. A. Laffey, Ph.D. Thesis, London, 1977.
- (32) A. H. Cooke, *Prog. Temp. Phys.*, **1**, 224 (1955).
- (33) We thank Mr. K. H. Bhatt for his technical assistance.

A Systematic X-Ray Absorption Study of Molybdenum Complexes. The Accuracy of Structural Information from Extended X-Ray Absorption Fine Structure

Stephen P. Cramer,^{1a} Keith O. Hodgson,^{*1a} Edward I. Stiefel,^{1b} and William E. Newton^{1b}

Contribution from the Department of Chemistry, Stanford University, Stanford, California 94305, and Charles F. Kettering Research Laboratory, Yellow Springs, Ohio 45387. Received June 30, 1977

Abstract: X-ray absorption spectra have been collected using synchrotron radiation for a number of mononuclear and dinuclear molybdenum complexes containing carbon, nitrogen, oxygen, and sulfur donor atoms. The extended fine structure (EXAFS) of the Mo absorption edge has been analyzed by a method which combines Fourier transform and curve-fitting techniques. Parameterized phase shift and amplitude functions for describing Mo-C, Mo-N, Mo-O, Mo-S, and Mo-Mo interactions were obtained from spectra of $Mo(CO)_6$, $Mo(NCS)_6^{3-}$, MoO_4^{2-} , $Mo(S_2C_6H_4)_3$, and $Mo_2O_4cys_2^{2-}$. Application of these phase shifts and amplitudes to the EXAFS of other compounds yielded distance determinations to an accuracy consistently better than 0.03 Å for atoms bound to Mo. The number and type of coordinating atoms were also determined with a reasonable degree of certainty. This work demonstrates the applicability (and limitations) of EXAFS for providing structural information about a specific absorbing center under noncrystalline conditions, and it lays a foundation for the analysis of the x-ray absorption spectra of nitrogenase and other Mo proteins.

Introduction

Recent experimental and theoretical advances have made x-ray absorption spectroscopy a promising new method for the study of local structure around a specific absorbing atom in metalloproteins,² catalysts,³ amorphous materials,^{4a} and many other cases where conventional diffraction methods are not feasible.^{4b} To this date, much of the work has centered on the determination of accurate absorber-scatterer distances. This in turn has caused a need for the evaluation of transferable phase shifts, whether by Fourier transform,⁵ curve fitting,⁶ or ab initio⁷ methods. At present, with highly symmetric structures involving only a single absorber-scatterer distance in the first coordination sphere, one can use any one of the above methods to obtain such distances to an accuracy of about 0.01 Å.

Besides radial distance information, EXAFS also contains information about the type and number of scattering atoms and their motion relative to the absorber. The atom type reveals itself through the absolute phase of the fine structure oscillations and through the EXAFS amplitude envelope. This amplitude is also affected by the static and thermal disorder of absorber-scatterer distances. Moreover, simple theory predicts that the magnitude of the fine structure will be linearly proportional to the number of scattering atoms and inversely proportional to the square of the absorber-scatterer distance. Until recently, much of the amplitude information has been discarded,⁸ but in this paper it is demonstrated that a set of transferable total amplitude functions can be used to determine the number of scatterers at a particular distance. Finally, the amplitude envelope and absolute phase shift together will be used to identify the elemental type(s) of scatterers involved.

For absorbers with unknown and/or complicated coordination spheres (several scattering elements and absorber-scatterer distances) one needs a systematic approach for extracting all the information contained in the extended fine structure. It is also essential to know the accuracy limits of the results obtained from this approach and to understand the major sources of error. In this paper, a general method for the quantitative analysis of the extended x-ray absorption fine structure (EXAFS) will be described. This method, shown schematically in Figure 1, is a hybrid of Fourier transform and curve-fitting techniques.

To test the reliability of this EXAFS analysis method, the extended fine structure spectra of a variety of molybdenum compounds have been measured and analyzed. Starting with relatively simple compounds of known structure, putatively transferable parameters for application of the method to Mo compounds in general have been derived. These parameters and the method were then used to determine bond distances of additional compounds whose structures had been elucidated previously by x-ray crystallography. The close correlation of both the distances and numbers of donor atoms derived by crystallographic and EXAFS evaluations of the same compounds lends confidence to our ability to predict donor atoms and distances in compounds of unknown structure. In subsequent papers this method will be used with model compound results to analyze the EXAFS of the molybdenum atoms in the nitrogenase enzyme and the metal sites of several other proteins.

Experimental Section

X-ray absorption spectra were obtained at the Stanford Synchrotron Radiation Laboratory (SSRL), using a Si[2,2,0] channel cut crystal monochromator and argon-filled ionization detectors.⁹ The typical available photon flux at 20 keV was on the order of 10^8 photons/s through a 2 cm \times 1 mm area. Computational work was done on a PDP 11/45 computer with a set of numerical analysis programs (called the XAP) written by Tom Eccles. These programs constitute a complete package of EXAFS analysis routines for small computer operation. They have been described briefly before,^{6a} and a more complete description will be published.¹⁰

The molybdate spectrum was measured on a freshly prepared 1 M aqueous solution of K_2MoO_4 (Research Organic/Inorganic Chemical Corp.) at neutral pH; identical first shell distances were obtained for solid hydrated Na_2MoO_4 from the same source. The thiomolybdate spectrum was obtained on a saturated aqueous solution of $(NH_4)_2MoS_4$, prepared by literature methods.^{11a} All other spectra were recorded on finely powdered solid samples using 0.25- or 0.5-mm path length cells. $Mo(CO)_6$ was obtained from Alfa/Ventron. The other compounds prepared for this study were $Mo(S_2C_6H_4)_3$,^{11b} $Mo(NHSC_6H_4)_3$,^{11c} $MoO(S_2CNET_2)$,^{11d} $Mo(S_2CNET_2)_2(S_2C_6H_4)$,^{11h} $Mo(S_2CNET_2)(S_2C_6H_4)_2$,^{11g} $MoO_2((SCH_2CH_2)_2NCH_2CH_2SMe)$,^{11e} $MoO_2((SCH_2CH_2)_2NCH_2CH_2NMe_2)$,^{11e} $MoO_3(dien)$,^{11f} $Na_2Mo_2O_4(cys)_2 \cdot 5H_2O$,¹² $Mo_2O_4(his)_2 \cdot 3H_2O$,^{13a} $Mo_2O_4(S_2CNET_2)_2$,^{13b} $Mo_2O_2S_2(SCNET_2)_2$,^{13c} $[(C_4H_9)_4N]_2Mo_2O_2S_2(i-mnt)_2$,^{13d} [*i-mnt* = 2,2-dicyanoethylene-1,1-dithiolate = $S_2CC(CN)_2$], $Mo(S_2CNET_2)_4$,^{14a} $(NH_4)_3Mo(NCS)_6 \cdot HCl \cdot H_2O$,^{14b} $Mo(CO)_2(S_2CNET_2)_2$,^{14c} and $Mo_2O_3(oxine)_2(SCH_2CH_2O)$.^{14d} Many of these compounds were kindly supplied by Drs. John W. McDonald and Narayanankutty Pariyadath of the Charles F. Kettering Research Laboratory.

Analysis Method

Phenomenologically, the extended fine structure is an oscillation in the absorption coefficient on the high-energy side of the absorption edge. The physical source for these oscillations is the scattering of the excited state outgoing photoelectron wave by neighboring atoms surrounding the central absorber.¹⁵ By making a number of approximations, one can arrive at a general expression for the EXAFS $\chi(k)$ in terms of calculable quantities:

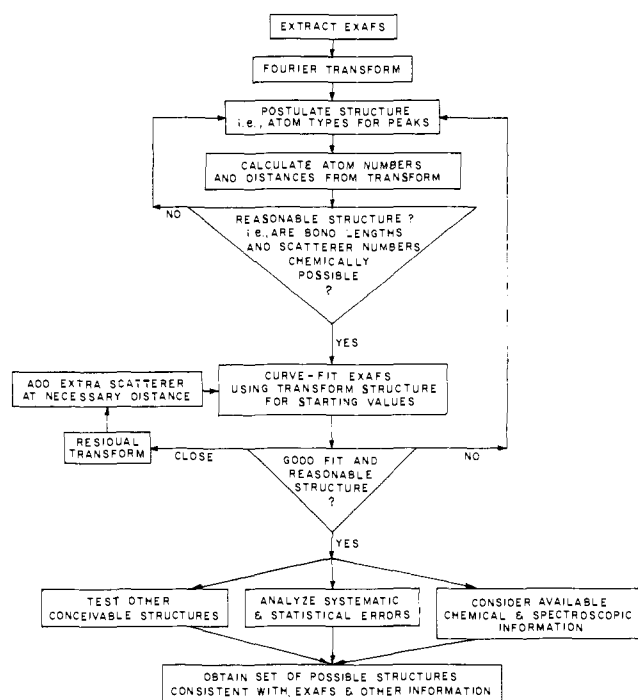


Figure 1. This flow chart represents one systematic procedure for going from the x-ray absorption spectrum of an unknown structure to a set of feasible coordination spheres. The precise method used will depend on the nature of the structural problem at hand. The residual transform is the Fourier transform of the difference between the calculated and observed EXAFS.

$$\chi(k) \equiv \frac{\mu - \mu_0}{\mu_0} = \frac{1}{k} \sum_s N_s \frac{f_s(\pi, k)}{R_{as}^2} \sin(2R_{as}) + \alpha_{as}(k) e^{-\sigma_{as}^2 k^2}$$

In this expression, μ is the observed absorption coefficient and μ_0 is the absorption coefficient in the absence of scattering neighbors. N_s is the number of scatterers at distance R_{as} from the absorber; $f_s(\pi, k)$ is the scatterer's electron backscattering amplitude; α_{as} is the total phase shift; σ_{as}^2 is the mean square deviation of R_{as} , and k is the photoelectron wave vector. The derivation of this expression^{5a,7e} is not extremely rigorous and involves a number of approximations which break down at low values of k (close to the absorption edge). Also, for scattering atoms beyond the first coordination sphere one must account for additional effects which diminish the photoelectron wave amplitude and/or change its phase as it propagates from the absorber. The results described herein show that regardless of the difficulties in theoretical calculation of these quantities, one can still describe the EXAFS of many structures by transferable empirical phase and amplitude functions.

This method of analysis is based on the assumption that the fine structure of a complicated system can be decomposed into a sum of individual absorber-scatterer interactions, and that the interactions can in turn be decomposed into phase shift and amplitude functions. These phase shifts and amplitudes could certainly be dismissed as meaningless fudge factors were it not for their successful transferability from one known structure to another with the accurate prediction of coordination numbers and bond lengths. The phase shifts and amplitudes to be used can be obtained by either Fourier transform or curve fitting methods, or by direct computation. They are essential for the quantitative interpretation of an EXAFS spectrum.

The procedure for structural determination from EXAFS can be summarized in a flow chart (Figure 1), the details of which will now be explained.

Isolation of EXAFS from the Absorption Spectrum. Unlike many other kinds of spectra, the extended fine structure is not

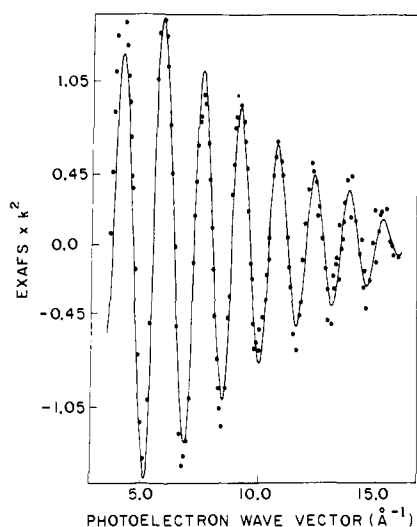


Figure 2. The effect of the Fourier filtering process on data for $\text{Mo}(\text{S}_2(\text{C}_6\text{H}_4)_3)_3$. The preliminary EXAFS data (solid points) were multiplied by k^3 , transformed from $k = 3.5 \text{ \AA}^{-1}$ to $k = 16.5 \text{ \AA}^{-1}$, retransformed from $R = 1.19 \text{ \AA}$ to $R = 2.69 \text{ \AA}$, and divided by k^3 . To aid in visualization, the EXAFS is amplified by k^2 in this and all other figures.

unambiguously determined. EXAFS is rather simply defined as $(\mu - \mu_S)/\mu_0$, where μ is the observed absorption coefficient of the atom type and edge of interest, μ_S is the smoothly varying part of that absorption, and μ_0 is the free atom absorption coefficient for that absorber unperturbed by scattering neighbors. However, μ_S is not experimentally observable, and the general assumption is that a smooth curve fitted to μ will closely approximate μ_S . Even determination of μ is not clear-cut, for besides the absorption of the element under study, there is still residual absorption by the other elements present and/or by the other edges of the same element. In a typical absorption experiment this monotonically decreasing background absorption is superimposed upon the energy dependence of the detector system (the spectrometer baseline). To further complicate matters, in fluorescence excitation experiments, a rising baseline (due to increasing sample penetration, increased Compton scattering, and reduced absorption of the scattering, as well as other effects) is actually observed. Thus, just extracting the fine structure from the experimentally recorded spectrum requires some effort.

In Figure 3 of ref 5b Lytle et al. described a procedure for obtaining the elemental absorption μ by extrapolation and subtraction of a Victoreen function in wavelength λ ($a\lambda^3 + b\lambda^4$) preedge. For the molybdenum spectra treated here, the absorption trend before the edge is sufficiently linear that subtraction of an extrapolated straight line preedge does a reasonable job of isolating the Mo K absorption. Considerable difficulty was encountered in using this extrapolation procedure at lower energy edges, however. An alternative to the extrapolation procedure is to normalize the absorption change (from below the edge to slightly beyond the edge) to unity. This will make $\mu_S = 1$. By assuming $\mu_S \cong \mu_0$, one can then scale the EXAFS by the known falloff of the absorption coefficient μ_0 . This removes the necessity of obtaining a good preedge extrapolation over the entire spectrum.

Subtraction of μ_S from μ (commonly termed "background subtraction") is conveniently done by means of a cubic spline routine. The absorption spectrum above the edge is divided into several regions, each of which is fit with a third-order polynomial, normally with a k^2 or k^3 weighting scheme. The individual polynomials are constrained to meet with equal slopes at the spline points, and combine to produce an overall curve for μ_S .

Another point of ambiguity in the extraction of the extended fine structure is the choice of E_0 , the x-ray energy corre-

sponding to zero photoelectron energy. The EXAFS is typically analyzed in terms of the photoelectron wave vector $k = (2m/\hbar^2(E - E_0))^{1/2}$ (E is the x-ray photon energy), and the choice of E_0 will affect the phase of the oscillations to be analyzed.

The E_0 has been consistently chosen as 20 025 eV, which is about 10 eV beyond the average of the highest inflection points of the apparent absorption edges. Examination of other choices for E_0 showed that the accuracy of the distances obtained was not significantly affected by the choice of E_0 , as long as the same E_0 was used throughout.

Fourier Transform. Once the normalized fine structure has been extracted from the absorption spectrum, it is Fourier transformed to reveal the major frequency components. Use of the Fourier transform to analyze EXAFS data was introduced by Sayers, Lytle, and Stern.^{5,16} They have shown that the major peaks in the transform correspond to the important absorber-scatterer distances, but shifted to lower R by a few tenths of an angstrom. In single-shell cases, or for multishell spectra involving well-isolated shells of scatterers, the transform method can provide quite accurate bond lengths and coordination numbers (see Tables IV-VI). However, for complicated absorber environments whose spectral transforms contain overlapping peaks, straightforward analysis of peak heights and positions becomes less accurate. In such cases, the transform can be used to extract a first best guess at the true structure. This guess is then refined using the curve-fitting methods presented later in this paper.

All of the transforms presented herein have been done by numerical integration over the range $k = 4-16 \text{ \AA}^{-1}$ using k^3 scaling. Although only the modulus of the transformed data has been presented, in principle the phase could be analyzed to yield information about the type of scatterer causing a given peak. Because such a phase analysis is impossible with overlapping transform peaks, the curve-fitting techniques discussed below were found necessary for identification of atom types in complicated structures.

The important quantities to be determined from the Fourier transforms of model compound spectra are (1) the effective phase shift α_{a-s}^* and (2) the effective per atom magnitude M_{a-s} . The effective phase shift is simply the difference between the observed Fourier transform peak position and the known absorber-scatterer distance, while the per atom magnitude is the observed peak height normalized to the number of scatterers and their distance:

$$\alpha_{a-s}^* = R_{a-s} - R_{\text{obsd}}$$

$$M_{a-s} = (M_{\text{obsd}}R_{a-s}^2)/N_s$$

Once these parameters have been obtained from known structures, they can be used to predict structures from the Fourier transforms of unknown spectra through simple inversion of these relations:

$$R'_{a-s} = R'_{\text{obsd}} + \alpha_{a-s}^*$$

$$N'_s = (R'_{a-s}M_{\text{obsd}})/M_{a-s}$$

Fourier Filtering. For curve-fitting analyses the data have been processed by a Fourier filtering procedure. The data (actually $k^3\chi(k)$ vs. k) were Fourier transformed (normally over $k = 3-17 \text{ \AA}^{-1}$) to R (frequency) space, then a region surrounding the peak(s) in the transformed spectrum was retransformed back to k space. Fourier filtering can cause some distortion of the fine structure, especially in the amplitude at the boundaries of the spectrum, but the use of relatively wide windows in both k and R space helps minimize these effects. The results of Fourier filtering the data for $\text{Mo}(\text{S}_2\text{C}_6\text{H}_4)_3$ are shown in Figure 2. Most of the distortion occurs as a decreased amplitude near the ends of the retransformed spectrum, and

for this reason a k space window wider than the fitting range was always used.

The advantages of Fourier filtering usually outweigh the problems of end point distortion. Fourier filtering provides a predetermined number of equally spaced points in k space. This means that one can oversample the spectrum during data collection and numerically smooth afterwards by means of the high-frequency cutoff. Furthermore, the low-frequency cutoff ensures removal of residual "background" which could otherwise distort the EXAFS baseline. Finally, in cases where the EXAFS is not rigorously single shell, one can sometimes isolate a peak of interest for fitting purposes, rather than trying to analyze the entire spectrum.

Curve Fitting. The first step in the curve-fitting operation is to empirically determine transferable functions for the total phase shift $\alpha_{as}(k)$ and the total scattering shell amplitude envelope $A_{as}(k)$

$$A_{as}(k) = |f_s(\pi, k)| e^{-\sigma_{as}^2 k^2}$$

for various absorber (a)-scatterer (s) pairs. The reliability and transferability of these phase shift and amplitude functions will be tested by the accuracy with which one can predict known structures. With the limits of error more fully established, one can then proceed to predict some unknown structures.

The empirical amplitude function used for EXAFS curve fitting was simply

$$A(k) \cong c_0 e^{-c_1 k^2} / k^{c_2}$$

The k^{c_2} factor was originally devised to model the electron-atom backscattering amplitude of light atoms (see Figure 11), while the exponential term was intended to be a Debye-Waller factor to account for thermal motion. Experience with a large number of fits has shown that these parameters are quite highly correlated (see Table II), so that it is impossible to make physical significance of either number separately. This is especially true when this total amplitude function is used to model EXAFS amplitudes of heavy scatterers such as Fe or Mo. However, the overall function gives an envelope magnitude and shape which is significant and promises to be transferable in cases of similar bonding.

For determination of scatterer numbers, the magnitude (c_0) and the shape parameters (c_1 and c_2) are first derived from curve fitting the spectra of model compounds. The latter two parameters are then held fixed, while the parameter c_0 , which determines the overall magnitude, is allowed to float freely in the unknown fit. By comparing the new c_0' of an unknown structure with the normalized c_0 obtained for a model, the number of scatterers in the unknown is calculated through

$$N' = c_0' R_{as}'^2 / c_0$$

It is clear from eq 1 that it is theoretically preferable to use integral scatterer numbers and to use a variable Debye-Waller factor to account for different amounts of thermal motion, and such procedures have been used previously. This can be done with the present functions simply by floating the c_1 parameter. This parameter is not intended to represent σ_{as}^2 in eq 1, since it also fits part of the backscattering amplitude. Thus, if the damping due to thermal motion is truly described by $e^{-\sigma_{as}^2 k^2}$, part of c_1 will reflect the backscattering amplitude envelope while the rest will reflect the mean square deviation of R_{as} :

$$c_1 = c_s + \sigma_{as}^2$$

where

$$|f(\pi, k)| \cong c_0 e^{-c_s k^2} / k^{c_2}$$

This dual role for c_1 explains why the current functional form for the total amplitude envelope can fit interactions with heavy

scatterers such as Mo, in which case the backscattering amplitude envelope peaks in the middle of a typical spectrum. Furthermore, by floating the c_1 parameter in a fit one can vary the relative Debye-Waller factor between the standard and the unknown. However, if the standard and the unknown have similar degrees of thermal motion, one can use a fixed c_1 and avoid this additional variable in the fits.

For absorber-scatterer distance determination, a simple quadratic polynomial was used to approximate the total phase shift:

$$\alpha_{as}(k) \cong a_0 + a_1 k + a_2 k^2$$

This total phase shift can be theoretically related to the sum of a backscattering phase shift (for reflection from the scattering atom) and a Coulomb phase shift (for propagation out of and back to the 1s hole). A different set of parameters for each Mo-X pair is obtained by curve fitting model compound spectra, as described below. Like the amplitude parameters, the phase shift parameters are highly correlated. Furthermore, they depend on the fitting range and are very sensitive to the choice of E_0 . Once the phase shift for a given Mo-X pair is known, unknown distances can be determined by fitting the oscillatory part of the unknown's EXAFS with the overall expression $\sin [a_0 + (2R_{a-s} + a_1)k + a_2 k^2]$, refining only the value of R_{a-s} .

For structures with N different scatterer types and/or bond lengths, a separate wave for each different Mo-X pair is needed. In general then, one optimizes $2N$ values when curve fitting an EXAFS spectrum. The N amplitude terms eventually yield the number of atoms of a given type, while the N phase terms give the absorber-scatterer distances.

With a completely unknown structure, one must also postulate the elemental type(s) of scatterer(s) contributing to the EXAFS, in order to apply the appropriate phase shift(s). Often, several different coordination spheres will be plausible from chemical information and the Fourier transform, in which case one must test each postulated structure by a curve-fitting refinement. There are thus two levels of iteration in the EXAFS analysis procedure: (1) refinement of scatterer numbers and distances for a postulated structure, and (2) refinement of the elemental identification of the scattering atoms contributing to the EXAFS. The application of this analysis procedure (Figure 1) will now be demonstrated on a variety of Mo structures.

Results

To obtain empirical parameters for the pairwise phase shift and amplitude functions, "single-shell" model compounds of known structure were employed when available. The term single shell refers to structures where (1) the absorbing atom is surrounded by a set of identical scatterers at nearly equal distances and (2) contributions to the EXAFS from more distant atoms are negligible. For Mo-O parameters, the molybdate ion (MoO_4^{2-}) in neutral aqueous solution was used (although almost identical results were obtained using solid hydrated sodium molybdate). Molybdenum tris(1,2-benzenedithiolate), $\text{Mo}(\text{S}_2\text{C}_6\text{H}_4)_3$, was used to obtain the Mo-S parameters. In both of these cases, there is only one significant peak in the Fourier transform of the EXAFS data.

For other Mo-X interactions, compounds were chosen where the contribution of a given shell could be cleanly isolated by Fourier filtering from the other components. Thus, for Mo-Mo parameters, the predominant peak in the Fourier transform of the molybdenum cysteine complex $\text{Na}_2(\text{MoO}_2\text{-O}_4\text{cys}_2) \cdot 5\text{H}_2\text{O}$ spectrum was analyzed. $(\text{NH}_4)_3\text{Mo}(\text{NCS})_6 \cdot \text{HCl} \cdot \text{H}_2\text{O}$ was used to obtain Mo-N parameters, while Mo-C parameters were obtained from the $\text{Mo}(\text{CO})_6$ spectrum.

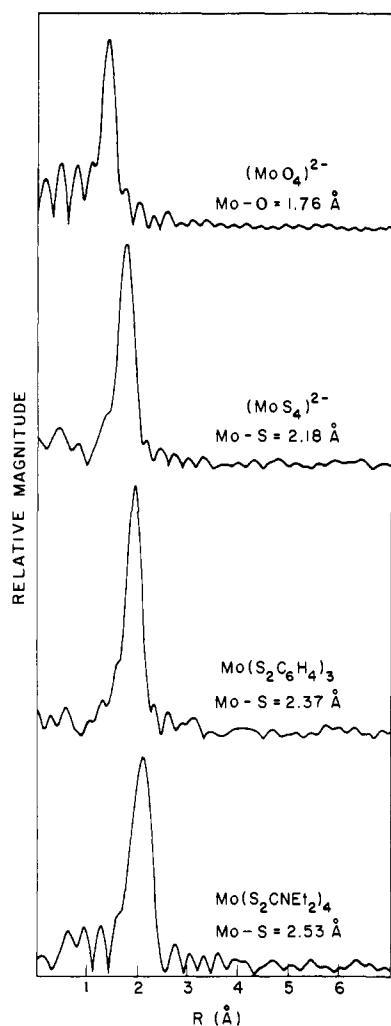


Figure 3. Fourier transforms of "single-shell" compounds. Curves show magnitude only. Transform range: 4–16 Å⁻¹, *k*³ scaling.

Fourier Transform Parameter Determination. The transforms of MoO₄²⁻ and Mo(S₂C₆H₄)₃ are shown in Figure 3, Mo(NCS)₆³⁻ and Mo(CO)₆ in Figure 10, and (Mo₂O₄cys₂)²⁻ in Figure 8. These model compound spectra provided values for the effective phase shift α^* and per atom magnitude *M* for the Mo–X interactions of interest, and these values are listed in Table I. The effective phase shifts show no obvious correlation with the atomic number of the scatterer, but they are more range dependent for the low *Z* scatterers. This range dependence of the effective phase shift is a reflection of the same phase shift nonlinearity which produces the low *R* shoulders on the transform peaks. The magnitude parameters are roughly proportional to *Z*, on the range of *k* = 4–12 Å⁻¹.

Curve Fitting for Parameter Determination. For curve-fitting analysis of the single-shell or pseudo-single shell models, the EXAFS of the above five compounds was Fourier filtered to isolate just the Mo–X interaction. Six parameter fits were then performed on the data using the functional form

$$\begin{aligned} \chi_{\text{Mo-X}}(k) &= \frac{N_X}{R^2} A_{\text{Mo-X}}(k) \sin [2kR + \alpha_{\text{Mo-X}}(k)] \\ &\cong \frac{N_X c_0 e^{-c_1 k^2}}{R^2 k^{c_2}} \sin [a_0 + (2R + a_1)k + a_2 k^2] \end{aligned}$$

Representative fitted and observed (filtered) spectra are shown in Figure 4 and the numbers derived from the fits are given in Table II.

In order to test the sensitivity of these empirical phase shift and amplitude functions to small changes of the fitting range

Table I. Fourier Transform Effective Phase Shifts and Magnitudes

Model		Transform range, Å ⁻¹		
		4–12	4–14	4–16
Mo(CO) ₆	$\alpha_{\text{Mo-C}}^*$	0.49	0.40	0.36
Mo–C = 2.06 Å	$M_{\text{Mo-C}}$	0.057	0.063	0.069
(ref 24)				
Mo(NCS) ₆ ³⁻	$\alpha_{\text{Mo-N}}^*$	0.47	0.43	0.43
Mo–N = 2.09 Å	$M_{\text{Mo-N}}$	0.065	0.075	0.080
(ref 21)				
(MoO ₄) ²⁻	$\alpha_{\text{Mo-O}}^*$	0.44	0.41	0.38
Mo–O = 1.76 Å	$M_{\text{Mo-O}}$	0.106	0.123	0.149
(ref 22)				
Mo(S ₂ C ₆ H ₄) ₃	$\alpha_{\text{Mo-S}}^*$	0.49	0.46	0.44
Mo–S = 2.37 Å	$M_{\text{Mo-S}}$	0.187	0.213	0.234
(ref 20)				
(Mo ₂ O ₄ cys ₂) ²⁻	$\alpha_{\text{Mo-Mo}}^*$	0.39	0.39	0.38
Mo–Mo = 2.57 Å	$M_{\text{Mo-Mo}}$	0.531	0.812	0.925
(ref 23)				

or the choice of *E*₀, both of these factors were systematically changed for the Mo(S₂C₆H₄)₃ fit. The various parameters arrived at from these nine fits are summarized in Table III. Inspection of this table makes it clear that no single parameter by itself is physically significant. Especially important to note is the sensitivity of the constant term, *a*₀, in the phase shift to small changes in the choice of *E*₀. Since *E*₀ (the threshold energy at which *k* = 0) is not experimentally determinable, it has been consistently fixed at 20 025 eV. This *E*₀ is 10 eV past the average highest edge inflection point of the Mo compounds examined.

One important feature of these single-shell spectra is the different amplitude envelopes observed for different types of scattering atoms. As expected, the oxygen amplitude dies out monotonically, while the sulfur amplitude peaks at relatively low *k* values and then dies away. The amplitude for the Mo–Mo wave clearly shows the EXAFS peaking at higher *k* values as the atomic number of the scatterer increases. (Note that all plots of fine structure have been multiplied by *k*² to make the higher *k* EXAFS visible.) The physical basis for this variation in EXAFS amplitude behavior is related to trends in the electron atom backscattering amplitudes, which peak at higher *k* values as *Z* increases⁸ (see Figure 11).

Single-Shell Tests of Transferability. As a first test of the transferability of the Mo–X parameters, the phase shifts and amplitudes were used to determine other known single-shell structures. The compounds chosen for this test, MoS₄²⁻ and Mo(S₂CNEt₂)₄, have different coordination numbers and different Mo–S distances from the model Mo(S₂C₆H₄)₃. To obtain structural information from the Fourier transform spectra of these compounds, the observed peak position *R*_{obsd} is simply modified by the previously determined phase shift $\alpha_{\text{Mo-S}}^*$ to obtain a predicted distance *R*_{Mo-S}. The coordination number is then obtained from the observed peak height. The predicted and crystallographically observed structural results are summarized in Table IV.

For curve-fitting analysis of the same spectra, two variables (*c*₀ and *R*_{Mo-S}) were floated while five were fixed (*c*₁, *c*₂, *a*₀, *a*₁, and *a*₂). This means that the shape of the amplitude envelope and the total phase shift have been fixed. The two terms floated yielded bond lengths and coordination numbers. The numerical results of these fits are presented in Table IV, and Figure 5 shows the fits themselves.

The results for single-shell fits indicate that the accuracy of absorber–scatterer distance determinations is on the order of 0.01 Å. Almost equal accuracy was obtained by use of the Fourier transform methods. The calculated coordination numbers, while correct to about 20%, did not show the same degree of accuracy as the distance calculations. This pre-

Table II. Curve-Fitting Phase Shift and Amplitude Parameters^a

optimized function: $(c_0 e^{-c_1 k^2} / k^{c_2}) \sin(a_0 + (2R + a_1)k + a_2 k^2)$; k^6 weighting

Model	Fitting range, Å ⁻¹	c_0	c_1	c_2	a_0	a_1	a_2
Mo(CO) ₆ Mo-C = 2.06 Å	4-12	0.0239	0.0317	-0.471	3.45	-1.966	0.0643
	4-14	0.0493	0.0260	0.0464	3.06	-1.854	0.0568
Mo(NCS) ₆ ³⁻ Mo-N = 2.09 Å	4-12	0.594	0.0178	1.482	4.01	-1.998	0.0674
	4-14	1.105	0.0126	1.952	3.03	-1.713	0.0479
(MoO ₄) ²⁻ Mo-O = 1.76 Å	4-12	1.172	0.00914	1.921	2.06	-1.541	0.0414
	4-14	1.692	0.00634	2.192	1.74	-1.441	0.0356
	4-16	1.802	0.00591	2.239	1.56	-1.406	0.0329
Mo(S ₂ C ₆ H ₄) ₃ Mo-S = 2.37 Å	4-12	0.641	0.0138	1.318	0.74	-1.717	0.0457
	4-14	0.884	0.0115	1.549	0.32	-1.598	0.0378
	4-16	0.923	0.0112	1.581	0.23	-1.574	0.0364
(Mo ₂ O ₄ cys ₂) ²⁻ Mo-Mo = 2.57 Å	4-12	0.00265	0.0176	-1.067	3.57	-1.207	0.0248
	4-14	0.00269	0.0175	-1.055	2.92	-1.051	0.0158
	4-16	0.00456	0.0156	-0.736	2.73	-1.009	0.0135

^a The c_0 values have not been normalized for N/R^2 .

Table III. Sensitivity of Parameters to Fitting Range and E_0

Model: Mo(S₂C₆H₄)₃, Inflection Point Energy 20 010.5 eV, Mo-S = 2.367 Å (ref 20)

optimized function: $(c_0 e^{-c_1 k^2} / k^{c_2}) \sin(a_0 + (2R + a_1)k + a_2 k^2)$; k^3 weighting

Parameter	$E_0 = 20\ 015.5$ eV fitting range, Å ⁻¹			$E_0 = 20\ 020.5$ eV fitting range, Å ⁻¹			$E_0 = 20\ 025.5$ eV fitting range, Å ⁻¹		
	4-12	4-14	4-16	4-12	4-14	4-16	4-12	4-14	4-16
c_0	0.289	0.398	0.472	0.274	0.370	0.428	0.315	0.393	0.445
c_1	0.0199	0.0170	0.0156	0.0196	0.0169	0.0156	0.0184	0.0162	0.0151
c_2	0.696	0.941	1.07	0.694	0.925	1.04	0.817	0.993	1.089
a_0	-1.25	-1.35	-1.37	-0.155	-0.304	-0.363	1.10	0.850	0.739
a_1	-1.43	-1.40	-1.40	-1.59	-1.55	-1.53	-1.80	-1.72	-1.69
a_2	0.0326	0.0304	0.0301	0.0402	0.0369	0.0357	0.0510	0.0451	0.0428

Table IV. Calculation of Single-Shell Distances and Coordination Numbers

Model: Mo(S₂C₆H₄)₃, Mo-S = 2.367 Å

Structure	Analysis range Å ⁻¹	Curve-fit distance, Å	Fourier transform distance, Å	Curve-fit no.	Fourier transform no.
(MoS ₄) ²⁻ Mo-S = 2.18 Å (ref 25)	4-12 ^a	2.179		4.15	
	4-12	2.179	2.19	4.56	4.3
	4-14	2.180	2.19	4.65	4.4
	4-16	2.180	2.19	4.65	4.5
Mo(S ₂ CNEt ₂) ₄ Mo-S = 2.529 Å (ref 26)	4-12 ^a	2.532		7.72	
	4-12	2.532	2.53	6.84	6.5
	4-14	2.533	2.53	6.56	6.4
	4-16		2.53		6.8

^a Floated $e^{-c_1 k^2}$.

sumably reflected neglect of the different amounts of thermal motion and/or disorder for the Mo-S bond lengths in MoS₄²⁻, Mo(S₂C₆H₄)₃, and Mo(S₂CNEt₂)₄. Thus, the calculations overestimate the number of sulfurs in the highly symmetric, tightly bound thiomolybdate case while underestimating the coordination number in the relatively loosely bound and less ordered dithiocarbamate complex.

To test the supposition that different degrees of thermal motion are the chief source of amplitude discrepancies, the single-shell fits were also performed with a floated $e^{-c_1 k^2}$ term. This extra degree of freedom, designed to reflect different Debye-Waller factors, dramatically improved the calculated number of atoms, but at the cost of an extra variable (see Table IV). Unfortunately, floating the c_1 parameter in the multishell fits described below did not improve the accuracy of the scatterer number calculations, and c_1 parameters were therefore

held fixed throughout the multishell fits. It is clear that empirical total amplitude functions are best transferable in cases where the thermal motion and the static spread in absorber-scatterer distances are similar.

Two-Shell Analysis. In order to test the hypothesis of EXAFS additivity and to gain experience with multishell fits, the compounds MoO(S₂CNEt₂)₂, Mo(C₆H₄NHS)₃, and MoO₃dien were examined. These were chosen for the presence of two distinctly different types of atoms bound to molybdenum. The Fourier transforms for these compounds are included in Figure 6, while their filtered EXAFS spectra and the corresponding fits are presented in Figure 7.

The Fourier transform spectra for these structures clearly show the presence of two different shells of scatterers. While the Mo-O and Mo-S interactions are clearly resolved in the MoO(S₂CNEt₂)₂ spectrum, for Mo(C₆H₄NHS)₃ the Mo-N

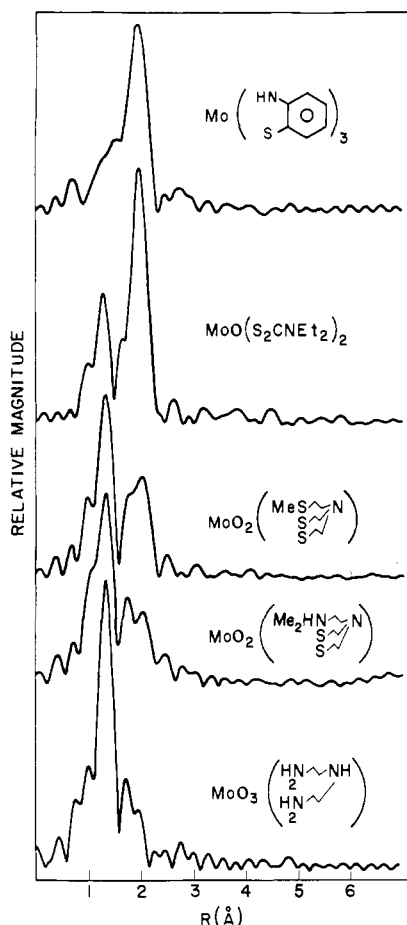


Figure 6. Fourier transforms of "multishell" compounds. Curves show magnitude only. Transform range: $4\text{--}16 \text{ \AA}^{-1}$, k^3 scaling.

The MoO_3dien structure is known,³¹ and comparison of the crystallographic and curve-fitting values shows that distances have been calculated to an accuracy of better than 0.01 \AA . The Fourier transform provides good numbers for Mo–O bond lengths and numbers. However, because the Mo–N peak is distorted by overlap with side lobes from the Mo–O peak, the transform Mo–N values are inaccurate and quite range dependent.

The $\text{Mo}(\text{C}_6\text{H}_4\text{NHS})_3$ structure is not known crystallographically; thus the obtained fit constitutes a structure prediction. The calculated sulfur number of 2.9 agrees well with the expected threefold sulfur coordination. The Mo–S distances appear to be nearly equal and centered at about 2.42 \AA . Similarly, the fits predict the presence of 3.2 nitrogens (3 expected) and average Mo–N distance of 2.00 \AA .

The results with two-shell fits were encouraging and informative. These fits are done assuming the additivity of fine structure, and this assumption appears valid in these test cases. In order to get meaningful numbers from curve fitting the fine structure, it was essential to minimize the number of refinable parameters. At this level of complexity, two such parameters per shell yielded very accurate distance ($\pm 0.02 \text{ \AA}$) and reasonably good scatterer numbers ($\pm 25\%$). To test the curve-fitting method even further, four-shell spectral analysis of several dinuclear Mo complexes was attempted.

Four-Shell Analysis. A set of di- μ -oxo and di- μ -sulfido bridged dinuclear Mo complexes was chosen for the next stage of analysis complexity. Spectra for Mo dimers are especially interesting because these structures have often been proposed as models for the active sites of molybdenum enzymes.³³ The Fourier transforms of the original EXAFS are presented in Figure 8. Representative Fourier-filtered spectra and the

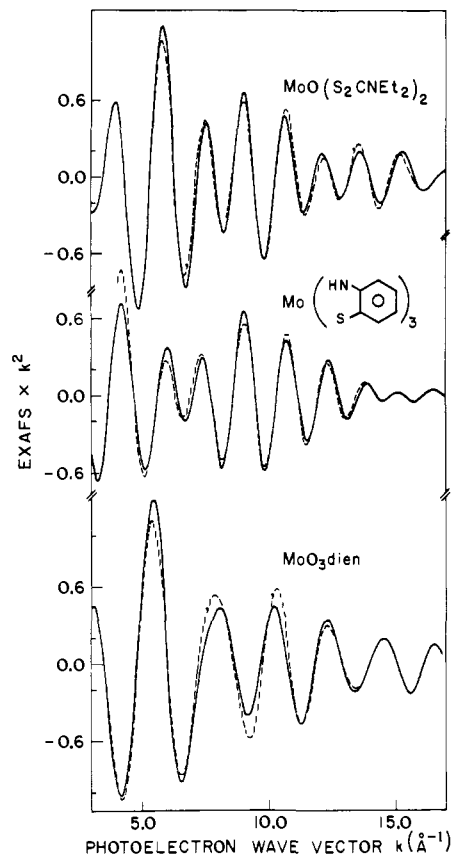


Figure 7. Two-shell fits for structure determination. The solid lines are filtered EXAFS and the dashed lines are least-squares fits.

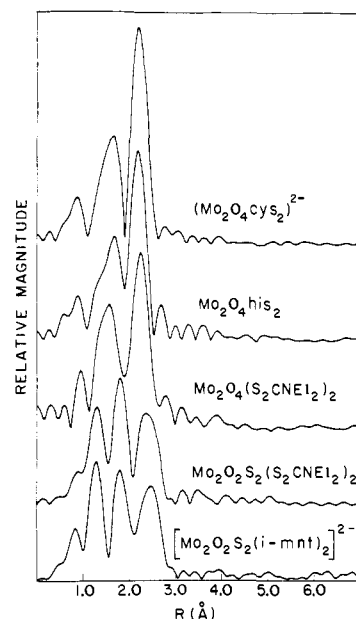


Figure 8. Fourier transforms of bridged dinuclear molybdenum complexes. Curves show magnitude only. Transform range: $4\text{--}16 \text{ \AA}^{-1}$, k^3 scaling.

corresponding fits are shown in Figure 9, and the calculated distances and coordination numbers are listed in Tables VI and VII.

A striking feature of all the Mo dimer transforms is the magnitude of the Mo–Mo peak. The large magnitude of this signal is due to a combination of a strong scatterer (Mo) and a low degree of thermal motion along the absorber–scatterer (Mo–Mo) bond axis.¹⁸ Attempts to observe metal–metal dis-

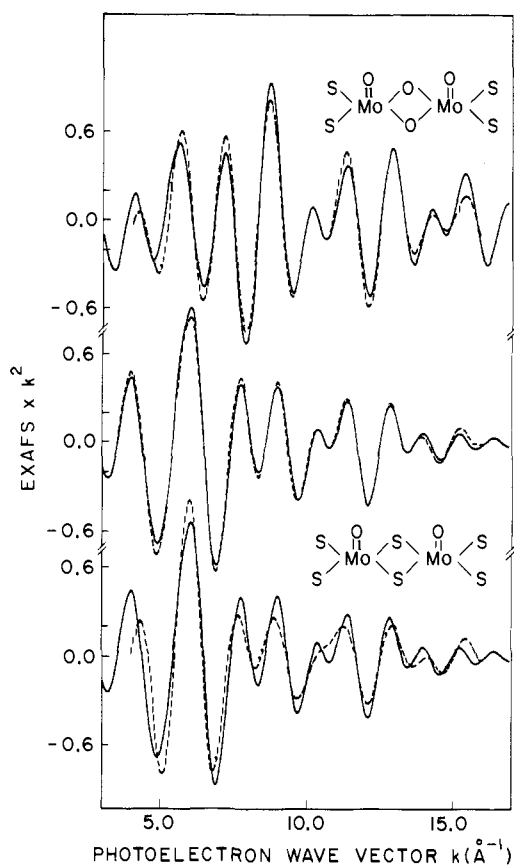


Figure 9. Four-shell fits for structure determination. The top solid line is the filtered EXAFS for $\text{Mo}_2\text{O}_4(\text{S}_2\text{CNET}_2)_2$, while the middle and bottom solid lines are the filtered EXAFS for $[\text{Mo}_2\text{O}_2\text{S}_2(i\text{-mnt})_2]^{2-}$. In the top two sets of curves, the dashed line is the least-squares fit using the correct parameters, while in the bottom set of curves the dashed line illustrates the result of incorrectly using Mo–O parameters for the Mo–Mo contribution to the EXAFS, while fitting the other three contributions correctly.

tances in other compounds have made it clear that bonding or rigid bridging between metals is almost essential for their interaction to be clearly observable in the fine structure.¹⁹ Fortunately, the combination of metal–metal bonding, tight bridging, and high scattering power makes the Mo–Mo interaction extremely distinctive in both original EXAFS and Fourier transformed data. The peak position is often an accurate measure of the Mo–Mo distance (see Table VI).

Further quantitative analysis of the Fourier-transformed data is frustrated by the overlap of different features. Terminal and bridging oxygens are unresolved for the oxo-bridged cases; similar overlap occurs for ligand and bridging sulfurs in the sulfido-bridged cases. Nevertheless, there is a clear difference between the Fourier transforms obtained for compounds containing the $\text{Mo}_2\text{O}_4^{2+}$ cores as compared to the $\text{Mo}_2\text{O}_2\text{S}_2^{2+}$ cores. Thus, despite the lack of resolution, the transform still reveals many of the important features of the first coordination sphere of molybdenum. Dimerization is shown clearly by the high R peak, while molybdenyl oxygen and coordinated sulfur also give peaks in characteristic regions.

Curve-fitting analysis of the dimer fine structure in k space provided greater resolution and more accurate scatterer numbers (see Figure 9 and Table VII). Four waves were included for the four distinctly different types of scattering atoms in the Mo coordination sphere. With variation of two parameters per shell (the amplitude c_0 and the R_{as} part of the frequency), this resulted in an eight-parameter fit. All eight of these parameters yielded quantitative structural information—distances and numbers of atoms. In most cases, correct

Table VI. Mo–Mo Distances by Fourier Transform
Phase Model: $[\text{Mo}_2\text{O}_4\text{cys}_2]^{2-}$, Mo–Mo = 2.569 Å

Structure	Crystallographic Mo–Mo, Å	Fourier transform EXAFS Mo–Mo, Å
$\text{Mo}_2\text{O}_4\text{his}_2 \cdot 3 \text{H}_2\text{O}$ (ref 30)	2.552	2.56
$\text{Mo}_2\text{O}_4(\text{S}_2\text{CNET}_2)_2$ (ref 28)	2.580	2.61
$\text{Mo}_2\text{O}_3(\text{oxime})_2(\text{SCH}_2\text{-CH}_2\text{O})$ (ref 14d)	2.628	2.63
$\text{Mo}_2\text{O}_2\text{S}_2(\text{S}_2\text{CNET}_2)_2$ (ref 29)	2.817	2.73
$[\text{Mo}_2\text{O}_2\text{S}_2(i\text{-mnt})_2]^{2-}$ (ref 13d)	2.821	2.83

identification of the elemental type of scatterer involved was also possible, for application of the wrong pairwise phase shift and amplitude functions will seriously diminish the quality of the fit. This is demonstrated at the bottom of Figure 9, where a Mo–O wave has been substituted for a Mo–Mo wave.

Inspection of the accuracy of the calculated distances shows that despite four different types of atoms in the first coordination sphere of molybdenum, the bond lengths were determined to an accuracy better than 0.03 Å. The calculation of scatterer numbers was considerably less precise, although it was always within an atom of being correct. The systematic errors were (1) overestimation of the number of molybdenyl oxygens, (2) underestimation of the number of ligand sulfurs, and (3) underestimation of the number of sulfido-bridged molybdenum atoms. These types of errors, although inevitable with the assumption of transferable total amplitude functions, can at least be rationalized as due to (1) tighter molybdenyl oxygen bonds than in the MoO_4^{2-} model,³² (2) slightly weaker Mo–S bonds with the dithiocarbamate ligands relative to the benzenedithiolate model,³⁴ and (3) less constraint on the Mo–Mo distance in the sulfido-bridged dimers compared with the oxo-bridged cysteine model. Obviously, for the best calculation of scatterer numbers, the model and unknown should have bonds of similar strength.

Structural Predictions. Demonstrating that an EXAFS analysis procedure gives accurate results with known structures is a necessary step in developing confidence with this procedure. However, an even more convincing test would be to predict structural results which could then be verified by x-ray crystallography. One such prediction has already been made for $\text{Mo}(\text{SNHC}_6\text{H}_4)_3$ in Table V. Additional structural predictions are now given for the compounds $\text{Mo}(\text{S}_2\text{CNET}_2)_2(\text{S}_2\text{C}_6\text{H}_4)$, $\text{Mo}(\text{S}_2\text{CNET}_2)(\text{S}_2\text{C}_6\text{H}_4)_2$, $\text{MoO}_2((\text{SCH}_2\text{CH}_2)_2\text{NCH}_2\text{CH}_2\text{SMe})$, and $\text{MoO}_2((\text{SCH}_2\text{CH}_2)_2\text{NCH}_2\text{CH}_2\text{NMe}_2)$. The results of curve-fitting analysis of the EXAFS of these compounds are presented in Table VIII.

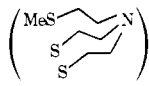
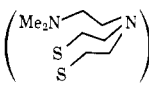
The two-shell fits on both all-sulfur ligand structures gave chemically reasonable bond lengths, and with appropriate rounding the calculated coordination numbers were correct. Deducing two distinct Mo–S distances from these fits was especially gratifying since the Fourier transforms gave only a single broad peak and the EXAFS itself does not show the strong beat pattern of the earlier two-shell fits.

Curve-fitting analysis of the tripod ligand complexes was significantly more difficult because of the variety of distances present and additional complications from the carbon backbone components. For $\text{MoO}_2((\text{SCH}_2\text{CH}_2)_2\text{NCH}_2\text{CH}_2\text{SMe})$, two strong components corresponding to two oxygens at 1.69 Å and two sulfurs at 2.40 Å were found. These should correspond to the doubly bound oxygens and the thiolate sulfurs, respectively. However, it was much more difficult to locate the nitrogen or thioether sulfur components, and the long Mo–S

Table VII. Four-Shell Fits of Molybdenum Dimers

Structure	Analysis	Mo-O ₊		Mo-X _{bridge}		Mo-S _{long}		Mo-Mo	
		Distance, Å	No.	Distance, Å	No.	Distance, Å	No.	Distance, Å	No.
Mo ₂ O ₄ (S ₂ CNEt ₂) ₂ (ref 28)	X-ray diff	1.679	1	1.941	2	2.455	2	2.580	1
	Fit 4-14 Å ⁻¹	1.667	1.2	1.939	1.9	2.440	1.3	2.574	0.9
	Fit 4-16 Å ⁻¹	1.670	1.3	1.939	1.9	2.445	1.5	2.578	1.0
Mo ₂ O ₂ S ₂ (S ₂ CNEt ₂) ₂ (ref 29)	X-ray diff	1.655	1	2.310	2	2.444	2	2.817	1
	Fit 4-14 Å ⁻¹	1.664	1.1	2.325	2.5	2.470	1.6	2.836	0.5
	Fit 4-16 Å ⁻¹	1.663	1.0	2.325	2.5	2.472	1.7	2.836	0.5
Mo ₂ O ₂ S ₂ (S ₂ C ₂ (CN) ₂) ₂ ²⁻ (ref 13d)	X-ray diff	1.663	1	2.296	2	2.434	2	2.821	1
	Fit 4-14 Å ⁻¹	1.657	1.4	2.323	2.3	2.457	1.6	2.834	0.6
	Fit 4-16 Å ⁻¹	1.678	1.3	2.322	2.1	2.458	1.7	2.834	0.6

Table VIII. Structure Prediction Fits^a

Structure	Mo-O ₊		Mo-S _{short}		Mo-S _{long}	
	Distance, Å	No.	Distance, Å	No.	Distance, Å	No.
Mo(S ₂ CNEt ₂) ₂ (S ₂ C ₆ H ₄)			2.314	2.2	2.424	3.6
Mo(S ₂ CNEt ₂)(S ₂ C ₆ H ₄) ₂			2.358	3.7	2.489	1.5
MoO ₂ 	1.693	2.1	2.401	1.7	2.803	0.5
MoO ₂ 	1.694	2.4	2.424	1.4		

^a All fits were over range of 4-14 Å⁻¹, *k*⁶ weighting.

Table IX. Collinearity Effects

Structure	Obscured shell			Analysis range, Å ⁻¹	FT distance, Å	FT no.	Curve-fit distance, Å	Curve-fit no.
	Element	Distance, Å	No.					
Mo(CO) ₆	O	3.18	6	4-12	3.12	9.4	3.07	9.6
				4-14	3.10	8.1	3.08	9.3
				4-16	3.11	8.7	3.09	9.1
Mo(CO) ₂ (S ₂ CNEt ₂) ₂	O	3.1 ^a	2	4-12	3.05	3.8	2.91	3.1
				4-14	2.96	4.2	2.96	2.6
				4-16	2.98	3.5		
(NH ₄) ₃ Mo(NCS) ₆ ·HCl·H ₂ O	C	3.23	6	4-12	3.17	8.4	3.13	8.0
				4-14	3.13	9.6	3.14	8.1
				4-16	3.14	8.8		

^a Estimated from similar structures.

distance of 2.80 Å is not as firm a prediction. A reasonable conclusion is that these latter two donor atoms are located trans to the Mo=O bonds and that their bonds to Mo are therefore considerably lengthened and weakened.

The other tripod ligand structure, MoO₂((SCH₂CH₂)₂-(NCH₂CH₂NMe₂)), appears to have even less regularity in its nonoxo bond lengths. The low value of 1.3 sulfurs (instead of 2) may reflect a sizable difference in the two Mo-S distances. It was difficult to predict the Mo-N distances with any confidence because of correlation problems.

Exceptional Cases. Quantitative analysis of EXAFS spectra by the curve-fitting method relies on several assumptions, one of which is the simple additivity of contributions from different sets of scatterers. For analysis of the absorber's first coordination sphere this additivity is a legitimate approximation. However, when analyzing more distant coordination spheres, other physical processes apart from electron-atom backscattering must be considered. When other atoms lie between the absorber and the scatterer of interest, one must take into account depletion of the primary outgoing wave as well as phase changes caused by the intervening atoms. Analysis of fine structure from the first coordination sphere can neglect such

effects, but for the study of more distant shells they can present distinct problems.

Two extreme cases of nonadditivity can be distinguished: (1) collinearity effects, where another atom is directly in line between the absorber and the scatterer of interest; and (2) depletion effects, in which case relatively large atoms occur in a nonlinear fashion between the absorber and the scatterer.

The effects of scatterer collinearity have been observed in many inorganic π -acceptor complexes, where di- or triatomic ligands (e.g., CO, NCS⁻, CN⁻) are linearly bound to the x-ray absorbing transition metal. Although one might intuitively expect atoms directly behind the first set of scatterers to have little contribution to the EXAFS, the opposite is actually true. This can be seen in the Fourier transforms of three π -bonded Mo complexes (Figure 10). The oxygens of the carbonyl ligands of Mo(CO)₂(S₂CNEt₂)₂ are clearly visible, as are both the carbons and the sulfurs of the isothiocyanate ligands of (NH₄)₃Mo(NCS)₆·HCl·H₂O. In Mo(CO)₆, the oxygen shell actually contributes more to the fine structure than does the inner shell of carbons.

Table IX summarizes the quantitative aspects of the colli-

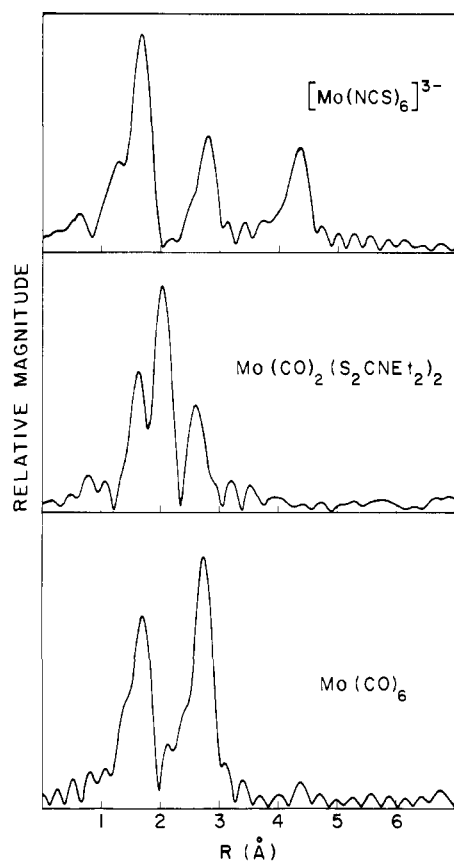


Figure 10. Collinearity effects. Presented are Fourier transform magnitudes for Mo compounds with shadowed second-shell scatterers. Transform range: 4–16 \AA^{-1} , k^3 scaling.

nearity effects. Using MoO_4^{2-} as a model, the observed contribution from the $\text{Mo}(\text{CO})_6$ carbonyl oxygens is about 50% greater than expected for a simple N/R^2 dependence. For $[\text{Mo}(\text{NCS})_6]^{3-}$, the carbon shell is also substantially stronger than expected. Furthermore, the next shell of sulfurs is clearly visible, at a distance (4.8 \AA) from which there is usually little contribution to the EXAFS. Still, it does not show enhancement over the N/R^2 formula, perhaps because of crystalline distortions from collinearity.²¹

Apart from these amplitude anomalies, obscured scatterers also tend to have different phase shifts from the line of sight cases. In curve fitting the obscured O and C shells in $\text{Mo}(\text{CO})_6$ and $[\text{Mo}(\text{NCS})_6]^{3-}$, respectively, it was necessary to vary the a_0 term in the phase shift to get a good fit. Furthermore, distances to obscured shells were underestimated 0.05–0.10 \AA , by both Fourier transform and curve-fitting procedures. These effects are evidence for an additional phase shift (which decreases with increasing k) due to the intervening scatterer. Similar anomalous phase shifts have been observed previously in the Fourier transform spectrum of Cu foil,^{7b} and they have been interpreted as the result of multiple scattering processes.

Amplitude Function Trends. For many experiments, it is useful to be able to estimate the relative magnitude of the effect a certain atom would produce on the EXAFS. Current theory predicts that the fine structure amplitude due to a particular scattering atom will be proportional to the electron-atom backscattering amplitude $|f(\pi, k)|$, but diminished by a Debye-Waller like factor $e^{-\sigma_{\text{as}}^2 k^2}$. In the high-energy limit, $|f(\pi, k)|$ is smoothly varying and ultimately proportional to Z , the atomic number of the scatterer, while at low energies $f(\pi, k)$ can show considerable structure. Conversely, differences in σ_{as} have a minor effect at low energies, but completely dominate the spectrum at high k values.

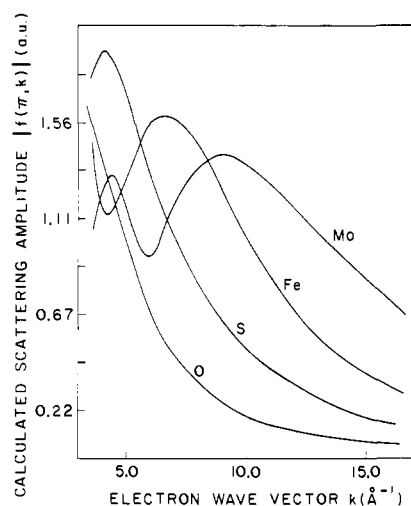


Figure 11. Theoretical electron-atom backscattering amplitudes. These curves are from a partial wave calculation using atomic potentials derived from Hartree-Fock wave functions.

In order to illustrate and quantitatively compare the dramatically different scattering amplitudes for low and high Z elements, values were obtained for $f(\pi, k)$ vs. k for O, S, Fe, and Mo. The calculations utilized the method of partial waves and Hartree-Fock atomic wave functions,¹⁷ and the results are presented in Figure 11. Since exchange and correlation effects have been neglected, these amplitudes are not as accurate as those of Lee and Beni.^{7c} Still, these curves are useful for illustrating the changes in shape and magnitude of $|f(\pi, k)|$ for different elements. For light atoms such as oxygen or sulfur $|f(\pi, k)|$ decreases rapidly, while heavier elements such as Fe and Mo show a pronounced peak in their scattering amplitudes at moderate k values. These calculations suggest that by careful analysis of EXAFS amplitudes, one should be able to distinguish between atoms in different regions of the periodic table. Low-temperature data collection is especially useful in this regard, for reduction of the thermal motion reduces the importance of the Debye-Waller factor and helps make the overall fine structure amplitude more characteristic of the scatterer.

It appears from Figure 11 that there might exist an intermediate k range where the scattering amplitudes are Z proportional, but Debye-Waller factors are not yet predominant, so that the EXAFS is directly proportional to the atomic number of the scatterer. To quantitatively test this idea, effective amplitudes per atom for C, N, O, S, and Mo were evaluated by both curve-fitting and Fourier transform methods. In the center of the range of a typical EXAFS spectrum (about $k = 8 \text{\AA}^{-1}$, or about 250 eV above E_0) the magnitude of the contribution by a given scatterer is linearly proportional to Z (see Tables I and II and Figure 12). This result holds whether one uses a Fourier transform from $k = 4$ to 12, or evaluates the empirical amplitude function at $k = 8$. However, at both low- and high-energy ends of the spectrum, this Z proportionality does not hold.

The low k EXAFS is quite sensitive to the shape of the scatterer's backscattering amplitude curve. At low energies, low Z atoms can actually backscatter more strongly than heavier atoms, and they will disproportionately affect the EXAFS in this regime. For example, at $k = 4 \text{\AA}^{-1}$, either Mo or S produces about the same magnitude effect on the fine structure.

At relatively high k values (high photoelectron energies), the EXAFS amplitude is extremely sensitive to thermal motion and disorder of the absorber-scatterer distances. If a relatively high Z scatterer is tightly bound to the absorber, it can domi-

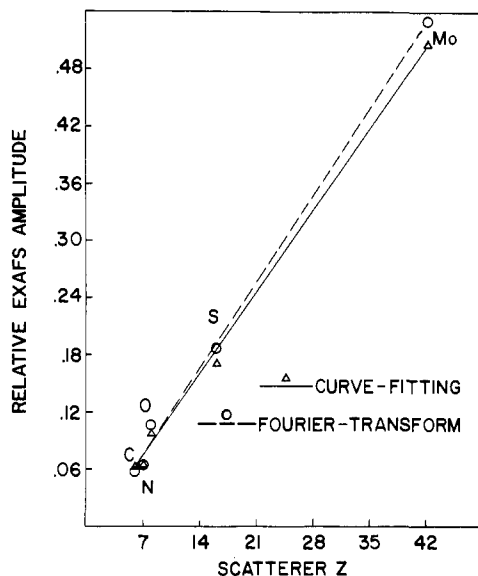


Figure 12. EXAFS amplitude vs. atomic number of scatterer. The circles represent the Fourier transform per atom magnitude $M_{\text{Mo-X}}$ for the 4–12 \AA^{-1} k range. The triangles are normalized parametrized amplitude functions evaluated at $k = 8 \text{\AA}^{-1}$ and multiplied by 10. The dashed and solid lines are linear least-squares fits to the data points.

nate the high-energy range of the spectrum. This is the case for the Mo–Mo interaction in the dinuclear spectra (Figure 9). Conversely, single metal–metal distances greater than 3 \AA are virtually impossible to see in the absence of some constraint on their relative thermal motion.¹⁹

Scatterer Identification through Phase Shifts. Theoretically, the total phase shift, α_{as} , can be treated as the sum of absorber and scatterer phase shifts:^{6b,9}

$$\alpha_{\text{as}}(k) = \alpha_{\text{a}}(k) + \alpha_{\text{s}}(k) - \pi$$

The absorber phase shift $\alpha_{\text{a}}(k) = 2\delta_1(k)$ is the result of the photoelectron propagating out of and back through the central atom potential. Reflection of the photoelectron by the scattering atom potential causes the scatterer phase shift $\alpha_{\text{s}}(k)$, and the final negative π is added to make the amplitude function positive.^{7d} Methods for ab initio calculation of these phase shifts have been discussed previously.^{7,9}

For a series of compounds with the same absorber, differences in total phase shifts are caused by the different α_{s} 's of the scattering atoms involved. Substantial differences in these total phase shifts were observed for the Mo models used for phase shift parametrization; these empirical pairwise phase shifts are shown in Figure 13. In accord with theoretical calculations,⁷ as the atomic number of the scatterer increases the mean value of the phase shift increases, while the average slope and curvature decrease.

The significant differences in phase shifts for O, S, and Mo permit straightforward differentiation between these atoms. Unless one uses the correct phase shift for a contribution to the EXAFS, the optimization procedure cannot produce an acceptable fit. Figure 5 shows the disastrous consequences of attempting to use a Mo–S phase shift for the Mo–O fine structure of $(\text{MoO}_4)^{2-}$. With multishell structures, as the complexity of the EXAFS increases and the fractional contribution by a given scatterer decreases, the differences between correct and incorrect atom identification become less dramatic (Figure 9). Still, even with four different component waves it was feasible to correctly identify O, S, and Mo contributions. On the other hand, it was difficult with the current data to distinguish between atoms with similar phase shifts, such as oxygen and nitrogen.

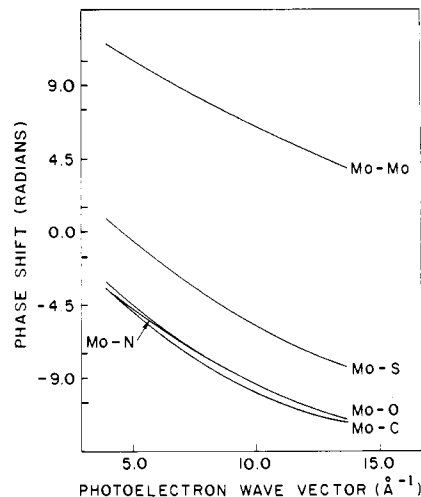


Figure 13. Empirical pairwise Mo–X phase shifts. Mo–S and Mo–Mo curves have been shifted vertically by 2π and 4π , respectively from values given by Table II parameters, in order to correspond to theoretical ordering.

Discussion and Summary

Although the existence of extended x-ray absorption fine structure has been known since the 1920s, it has only been within the past few years that structural predictions from EXAFS have become at all reliable. As a new technique with much potential, it has stimulated many claims and much controversy as to what EXAFS analysis can or cannot do. The significance of this present work is that it describes a coherent approach for the analysis of complicated coordination spheres using a methodology whose accuracy has been thoroughly tested on a number of known structures. Thus, it lays the groundwork for the prediction of unknown structures such as the environment of molybdenum in nitrogenase and other molybdenum-containing enzymes.

In this work, a series of molybdenum complexes with 1, 2, and 4 characteristic absorber–scatterer distances were systematically studied. For single-shell structures, distance determinations with an accuracy better than 0.01 \AA were obtained. Furthermore, using roughly transferable total amplitude functions, coordination number calculations with better than 15% accuracy were possible. However, such single-shell structures are rarely of chemical interest.

For “multishell” structures, distance determinations with an accuracy of 0.03 \AA were always achieved, and comparison of the 16 distances calculated from EXAFS (over 4–14 \AA^{-1}) with the x-ray crystallographic values yields an average deviation of 0.012 \AA . Since only two parameters per scatterer type are refined (R_{as} for the distance and c_0 for the number of scatterers) the correlation between parameters is kept to a minimum.

With the current method of analysis, the calculation of scatterer numbers is less accurate than the distance determinations, although it is normally correct to within an atom. The average percentage deviation for the calculated number of scatters of a given type was 19%, for 18 different scatterers analyzed in multishell fits on the range of 4–14 \AA^{-1} . The accuracy is primarily limited by the sensitivity of the fine structure to thermal motion and static variations in absorber–scatterer distances. By adjusting the amplitude envelope parameters for different Debye–Waller factors the single-shell numbers can be improved, but such extra variable parameters did not improve the accuracy of multishell fits. For good predictions of scatterer numbers using empirical amplitude functions, models with bonding similar to the structure under study should be used.

A continuing controversy has existed over the relative merits of curve-fitting and Fourier transform analysis methods. The transform procedure has been criticized for giving false peaks and yielding range and weighting-dependent phase shifts. The single-shell transforms of Figure 3 illustrate the lower R shoulders on primary peaks (caused by phase shift nonlinearity) and the side lobes (a cutoff effect) typical of most EXAFS Fourier transforms. Although these features prevent the transform magnitude from truly representing a radial distribution function, they do not prevent analysis of the absorber's coordination sphere, once one is accustomed to their appearance. Thus, single-shell molybdenum-sulfur distances were calculated with 0.01 Å accuracy, while two-shell distance determinations were generally within 0.1 Å.

The present experience with multishell Fourier transforms shows that their primary source of error stems from overlapping peaks rather than phase shift nonlinearity or cutoff effects. When different sets of scatterers have overlapping transform peaks, interference between the transform components distorts the magnitude envelope in a complicated manner, and simple peak heights and positions become unreliable structural indicators. Curve fitting the EXAFS directly in k space avoids this problem, and curve-fitting analysis is preferred when the Fourier transform shows evidence of unresolved components.

At this point, the potential and the limitations of EXAFS analysis are becoming clearer. The data presented here show that the extended fine structure can be used to characterize the number, atomic type, and distances of scattering atoms within the absorber's first coordination sphere. The accuracy of the calculated structure varies inversely with the number of different scatterers contributing to the EXAFS, and therefore simpler structures are more amenable to analysis than are highly asymmetric ones. In many transition metal complexes, atoms beyond the first coordination sphere contribute little to the EXAFS, and one thus has an extremely local view of the absorber's environment. This invisibility of more distant shells can often simplify the analysis required.

In the present study, 20 mono- and dinuclear complexes of molybdenum were investigated, of which 14 had known structures. Five of the compounds were used to set values for Mo-C, Mo-N, Mo-O, Mo-S, and Mo-Mo scattering parameters and these were then used to derive values for bond distances in the remaining compounds. In each of the nine cases where crystallographic information was available, the EXAFS-derived distances correlated very closely to those derived by x-ray determination. Qualitatively it is clearly possible to distinguish mononuclear from dinuclear sites, the presence of S compared to O as bridging or ligand donor atoms, and the presence or absence of terminal oxo groups. Successful analysis of known structures led to specific predictions for those cases where crystallographic information was not available.

Analysis of the extended fine structure can never give a complete structural picture, for the EXAFS normally does not reveal geometry or stereochemistry. It is also difficult to identify single light scatterers present simultaneously with a group of heavy, tightly bound ligands (for example, a water molecule loosely coordinated to a metal with several sulfur ligands). Finally, scattering atoms of the same element with distances less than about 0.05 Å apart cannot be resolved. Thus, for the analysis of completely unknown structures such as the molybdenum sites in metalloenzymes, EXAFS will often suggest a set of possible coordination spheres rather than a unique structure. Despite this limitation, EXAFS analysis can provide a great deal of information currently unobtainable by any other method. Continuing improvements in both analysis methodology and experimental sensitivity should make EXAFS an important tool in many future structural investigations.

Acknowledgments. We would like to acknowledge Sebastian Doniach for helpful discussions about this analysis and for his continued encouragement. We would also like to thank Drs. John McDonald and Narayanankutty Pariyadath for their generous donation of a number of Mo compounds used in this study. We thank Ms. Sue Sperlich for synthesizing many useful models as well. We are pleased to acknowledge Dr. Milan Blaha for the theoretical amplitude calculations. Finally, we thank Dr. Thomas Eccles for the computer programming of both data collection and data analysis packages; without this contribution, the current work could not have been done. K.O.H. is a Fellow of the Alfred P. Sloan Foundation and S.P.C. was an IBM Doctoral Fellow for 1976-1977. This work was supported by the National Science Foundation through Grant PCM-75-17105. Synchrotron radiation time was provided by the Stanford Synchrotron Radiation Laboratory, supported by the National Science Foundation Grant DMR-07692-A02 in cooperation with the Stanford Linear Accelerator Center and the Energy Research and Development Administration.

References and Notes

- (1) (a) Stanford University; (b) Charles F. Kettering Research Laboratory.
- (2) (a) B. M. Kincaid, P. M. Eisenberger, K. O. Hodgson, and S. Doniach, *Proc. Natl. Acad. Sci. U.S.A.*, **72**, 2340 (1975); (b) R. G. Shulman, P. Eisenberger, W. E. Blumberg, and N. A. Stombaugh, *Ibid.*, **72**, 4003 (1975); (c) P. Eisenberger, R. G. Shulman, G. S. Brown, and S. Ogawa, *Ibid.*, **73**, 491 (1976); (d) V. W. Hu, S. I. Chan, and G. S. Brown, *Ibid.*, **74**, 3821 (1977).
- (3) (a) F. W. Lytle, D. E. Sayers, and E. B. Moore, *Appl. Phys. Lett.*, **24**, 45 (1974); (b) I. W. Bassi, F. W. Lytle, and G. Parravano, *J. Catal.*, **42**, 139 (1976); (c) J. Reed, P. Eisenberger, B. K. Teo, and B. M. Kincaid, *J. Am. Chem. Soc.*, **99**, 5217 (1977).
- (4) (a) S. Hunter, Ph.D. Thesis, Stanford University, 1977. (b) For a review of x-ray absorption spectroscopy prior to synchrotron radiation, see L. Azaroff and D. Pease in "X-Ray Spectroscopy", L. Azaroff, Ed., McGraw-Hill, New York, N.Y., 1974, Chapter 5. A review of recent work at SSRL is in press: S. P. Cramer and K. O. Hodgson, *Adv. Inorg. Chem.*, in press.
- (5) (a) E. Stern, *Phys. Rev. Sect. B*, **10**, 3207 (1974); (b) F. W. Lytle, D. E. Sayers, and E. A. Stern, *Ibid.*, **11**, 4825 (1975); (c) E. A. Stern, D. E. Sayers, and F. W. Lytle, *Ibid.*, **11**, 4836 (1975).
- (6) (a) S. P. Cramer, T. K. Eccles, F. Kutzler, K. O. Hodgson, and S. Doniach, *J. Am. Chem. Soc.*, **96**, 8059 (1976); (b) P. H. Citrin, P. Eisenberger, and B. M. Kincaid, *Phys. Rev. Lett.*, **36**, 1346 (1976).
- (7) (a) B. M. Kincaid and P. Eisenberger, *Phys. Rev. Lett.*, **34**, 1361 (1975); (b) P. A. Lee and J. B. Pendry, *Phys. Rev. Sect. B*, **11**, 2795 (1975); (c) P. A. Lee and G. Beni, *Ibid.*, **15**, 2862 (1977); (d) P. A. Lee, B. K. Teo, and A. L. Simons, *J. Am. Chem. Soc.*, **99**, 3856 (1977); (e) C. A. Ashley and S. Doniach, *Phys. Rev. Sect. B*, **11**, 1279 (1975).
- (8) Recently, progress in parametrization of theoretical amplitude curves has been reported: B. K. Teo, P. A. Lee, A. L. Simons, P. Eisenberger, and B. M. Kincaid, *J. Am. Chem. Soc.*, **99**, 3854 (1977). Analysis of amplitude data is also discussed in ref 5b and 5c.
- (9) B. M. Kincaid, Ph.D. Thesis, Stanford University, 1974.
- (10) T. K. Eccles, Ph.D. Thesis, Stanford University, 1977.
- (11) (a) A. Muller, and E. Diemann, *Chem. Ber.*, **102**, 2603 (1969); (b) E. I. Stiefel, R. Eisenberg, R. C. Rosenberg, and H. B. Gray, *J. Am. Chem. Soc.*, **88**, 2956 (1966); (c) J. K. Gardner and E. I. Stiefel in Proceedings First International Conference on Chemistry and Uses of Molybdenum, P. C. H. Mitchell, Ed., Climax Molybdenum Co., 1973; *J. Less-Common Met.*, **36**, 521 (1974); J. K. Gardner, N. Pariyadath, J. L. Corbin, and E. I. Stiefel, *Inorg. Chem.*, in press; (d) R. N. Jowitt and P. C. H. Mitchell, *J. Chem. Soc. A*, 2631 (1969); (e) N. Pariyadath, J. L. Corbin, and E. I. Stiefel, to be published; (f) W. F. Marzluff, *Inorg. Chem.*, **3**, 395 (1964); (g) W. E. Newton, G. J.-J. Chen, and J. W. McDonald, *J. Am. Chem. Soc.*, **98**, 5387 (1976); (h) J. W. McDonald, G. J.-J. Chen, and W. E. Newton, manuscript in preparation.
- (12) A. Kay and P. C. H. Mitchell, *J. Chem. Soc. A*, 2421 (1970).
- (13) (a) L. R. Melby, *Inorg. Chem.*, **8**, 1539 (1969); (b) W. E. Newton, J. L. Corbin, D. C. Bravard, J. E. Searles, and J. W. McDonald, *Ibid.*, **13**, 1100 (1974); (c) V. R. Ott, D. S. Rollison, F. A. Schultz, J. W. McDonald, and W. E. Newton, submitted for publication; (d) J. Gelder and J. H. Enemark, *Inorg. Chem.*, **15**, 1839 (1976).
- (14) (a) Z. B. Varadl and A. Nieuwpoort, *Inorg. Nucl. Chem. Lett.*, **10**, 801 (1974); (b) J. Lewis, R. S. Nyholm, and P. W. Smith, *J. Chem. Soc.*, 4590 (1961); (c) R. Colton, G. R. Scollary, and I. B. Tomkins, *Aust. J. Chem.*, **21**, 15 (1968); J. W. McDonald, W. E. Newton, C. T. C. Creedy, and J. L. Corbin, *J. Organomet. Chem.*, **92**, C25 (1975); (d) J. I. Gelder, J. H. Enemark, G. Wolterman, D. A. Boston, and G. P. Haight, *J. Am. Chem. Soc.*, **97**, 1616 (1975).
- (15) For a qualitative description of the physics involved in the EXAFS effect, see E. Stern, *Sci. Am.*, **234**, 96 (1976).
- (16) D. E. Sayers, F. W. Lytle, and E. A. Stern, *Adv. X-Ray Anal.*, **13**, 248 (1970).
- (17) E. Clementi, *IBM J. Res. Dev.*, **9**, 2 (1965).
- (18) The low degree of thermal motion along the Mo-Mo axis has been remarked upon in ref 23.
- (19) Attempts to observe nonbonded Ni-Ni distances of about 3 Å were not successful: F. W. Kutzler, unpublished results. Similar difficulties were

- encountered in observation of nonbonded Cu-Cu distances (ref 10).
- (20) M. Cowie and M. J. Bennett, *Inorg. Chem.*, **15**, 1584 (1976).
- (21) J. R. Knox and K. Eriks, *Inorg. Chem.*, **7**, 84 (1968).
- (22) B. M. Gatehouse and P. Leverett, *J. Chem. Soc. A*, 849 (1969).
- (23) J. R. Knox and C. K. Prout, *Acta Crystallogr., Sect. B*, **25**, 1857 (1969).
- (24) G. M. Nadarian, Ph.D. Thesis, California Institute of Technology, 1957.
- (25) (a) H. Schäfer, G. Schäfer, and A. Weiss, *Z. Naturforsch. B*, **19**, 76 (1964); (b) W. P. Binnie, M. J. Redman, and W. J. Mallico, *Inorg. Chem.*, **9**, 1449 (1970); (c) P. A. Koz'min and Z. V. Popova, *Zh. Strukt. Khim.*, **12**, 99 (1971).
- (26) J. G. M. van der Aalsvoort and P. T. Bevrskens, *Cryst. Struct. Commun.*, **3**, 653 (1974).
- (27) L. Ricard, J. Estienne, P. Karagiannidis, P. Toledano, J. Fischer, A. Mitschler, and R. Weiss, *J. Coord. Chem.*, **3**, 277 (1974).
- (28) L. Ricard, C. Martin, R. Wiest, and R. Weiss, *Inorg. Chem.*, **14**, 2300 (1975).
- (29) R. Winograd, B. Spivack, and L. Dori, *Cryst. Struct. Commun.*, **5**, 373 (1976).
- (30) L. T. J. Delbaere and C. K. Prout, *Chem. Commun.*, 162 (1971).
- (31) F. A. Cotton and R. C. Elder, *Inorg. Chem.*, **3**, 397 (1964).
- (32) E. I. Stiefel, *Prog. Inorg. Chem.*, **22**, 1 (1977).
- (33) E. I. Stiefel, W. E. Newton, G. D. Watt, K. L. Hadfield, and W. A. Bulen, "Bioinorganic Chemistry-II", *Adv. Chem. Ser.*, **162**, 353 (1977).
- (34) R. Eisenberg, *Prog. Inorg. Chem.*, **12**, 295 (1970).

Oxygen Binding to Cobalt Porphyrins

James P. Collman,*¹ John I. Brauman, Kenneth M. Doxsee, Thomas R. Halbert, Susan E. Hayes, and Kenneth S. Suslick

Contribution from the Department of Chemistry, Stanford University, Stanford, California 94305. Received August 3, 1977

Abstract: The thermodynamic constants of oxygen binding to cobalt "picket fence" porphyrin complexes, *meso*-tetra($\alpha,\alpha,\alpha,\alpha$ -*o*-pivalamidophenyl)porphyrinatocobalt(II)-1-methylimidazole and 1,2-dimethylimidazole, are reported. In contrast to previously studied cobalt porphyrins, these complexes bind oxygen with the same affinity as cobalt substituted myoglobin and hemoglobin. Solvation effects are discussed as the source of this difference. The use of sterically hindered axial bases as models of T state hemoglobin is discussed.

In studies of myoglobin (Mb) and hemoglobin (Hb), the replacement of the neutral iron porphyrin prosthetic group with different metalloporphyrins has proved to be a useful technique.² Artificial hemoglobins containing zinc,^{2,3} manganese,⁴⁻⁸ copper,⁴ and nickel⁹ have been reconstituted, and their properties compared with those of the native iron proteins. These artificial systems, however, are incapable of reversible oxygenation. In contrast, cobalt substituted hemoglobin and myoglobin (CoHb and CoMb)¹⁰ are functional,¹¹⁻¹³ although their oxygen affinities are 10-100 times less than those of native Hb and Mb.

CoHb exhibits cooperativity in oxygen binding, though to a lesser degree than Hb. The extent of this cooperativity is conveniently expressed as ΔG_{41}° , the free energy difference between the intrinsic binding of the first and the fourth O₂ to Hb.^{13b,c} For CoHb, ΔG_{41}° is roughly one-third that of Hb under comparable conditions.^{13b} Because of the different stereochemical and electronic factors involved in binding oxygen to a cobalt porphyrin, the observation of cooperativity in CoHb has been variously used either to question^{2,12,14} or support^{13b,15} the elegant proposal of Perutz concerning the molecular mechanism of cooperativity in natural Hb.¹⁶ At the heart of this proposal is the assumption, based on earlier ideas of Hoard¹⁷ and Williams,¹⁸ that the high-spin iron in the unligated, low O₂ affinity form of Hb (T state) lies out of the porphyrin plane, and that on binding O₂, the iron becomes low spin and moves into the plane. The resulting motion of the proximal imidazole (0.6 Å) then causes conformational changes in the protein which produce a higher O₂ affinity quaternary form of the protein (R state). In the deoxy form of coboglobin, cobalt is low spin rather than high spin and the best estimates from simple cobalt model systems indicate that the proximal imidazole in CoHb moves ~0.4 Å upon oxygenation^{14,19,20} as opposed to the 0.6 Å for Hb. The resulting motion of the proximal histidine upon binding O₂ will therefore only be two-thirds as great. This seems to be qualitatively consistent with the lowered ΔG_{41}° of CoHb.

This same reasoning argues that a real tension of the Co-

N_{HIS} bond may exist in the deoxy (T) form of CoHb. The best current explanation of cooperativity is a "restraint" theory:^{15a} by holding the proximal imidazole in place, the T form of the native protein restrains the five-coordinate, deoxy metalloporphyrin from becoming six coordinate, *without* necessarily inducing any strain in the deoxy form of native Hb itself. In deoxy CoHb, however, the Co atom is already closer to the mean porphyrin plane than is Fe and is likely to have created a real strain in the Co-N_{HIS} bond, which would be demonstrated as a lengthening of this bond as in structures of CoTPP(1,2-diMeIm)¹⁰ compared with CoTPP(N-MeIm).^{10,19}

In an effort to further clarify the nature of O₂ binding to CoHb, and, by implication, to native Hb, many workers in the last several years have investigated the reaction of simple cobalt(II) porphyrins with oxygen.^{2,11,21-29} This work has been frustrated in most cases to date by the surprisingly low affinity of such simple cobalt(II) porphyrins for oxygen in the absence of the globin protein environment. For example, whereas CoHb has $P_{1/2}^{O_2}$ (22 °C) of 50 Torr, CoT-*p*-OCH₃PP(*N*-MeIm)¹⁰ in toluene has $P_{1/2}^{O_2}$ (25 °C) of 15 500 Torr.³⁰

In a previous paper,²⁸ the synthesis of the cobalt derivative of the "picket fence" porphyrin, CoTpivPP (1 in Figure 1) was reported, along with its *N*-methylimidazole (*N*-MeIm) adduct, **2**. It was pointed out that the five-coordinate cobalt porphyrin **2** has a fairly high O₂ affinity at room temperature in solution, but no thermodynamic data were obtained. We have since found that the method previously used for introduction of cobalt into the "picket fence" porphyrin resulted in rotation of the pivalamidophenyl groups ("pickets") to give a statistical mixture of atropisomers, and have therefore developed a milder technique that does not cause this rotational isomerization. In this paper, we report the improved synthesis, along with the thermodynamic constants for oxygen binding to CoTpivPP(*N*-MeIm), **2**, in the solid state and in solution. In the solid state and in toluene, this simple porphyrin is found to bind oxygen as well as CoMb. In addition, a decrease in oxygen affinity has been observed when *N*-MeIm is replaced by a